FRONTIERS OF PHYSICS

RESEARCH ARTICLE
Volume 18 / Issue 1 / 12303 / 2023

Dynamic polarization rotation and vector field steering based on phase change metasurface

Hairong He, Hui Yang, Zhenwei Xie†, Xiaocong Yuan

Nanophotonics Research Center, Shenzhen Key Laboratory of Micro-scale Optical Information Technology, Institute of Microscale Optoelectronics, Shenzhen University, Shenzhen 518060, China
Corresponding author. E-mail: †ayst3_1415926@sina.com
Received June 1, 2022; accepted September 15, 2022

ABSTRACT

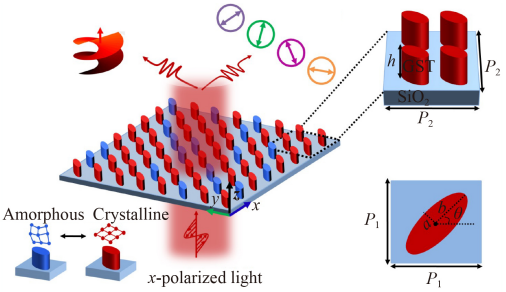

Polarization rotation and vector field steering of electromagnetic wave are of great significance in modern optical applications. However, conventional polarization devices are bulky, monofunctional and lack of tunability, which pose great challenges to the miniaturized and multifunctional applications. Herein, we propose a meta-device that is capable of multi-state polarization rotation and vector field steering based on phase change metasurface. The supercell of the meta-device consists of four $Ge_2Sb_2Te_5$ (GST) elliptic cylinders located on a SiO_2 substrate. By independently controlling the phase state (amorphous or crystalline) of each GST elliptic cylinder, the meta-device can rotate the polarization plane of the linearly polarized incident light to different angles that cover from 19.8° to 154.9° at a wavelength of 1550 nm. Furthermore, by merely altering the phase transition state of GST elliptic cylinders, we successfully demonstrated a vector field steering by generating optical vortices carrying orbital angular momentums (OAMs) with topological charges of 0, 1 and –1, respectively. The proposed method provides a new platform for investigating dynamically tunable optical devices and has potential applications in many fields such as optical communications and information processing.

Keywords polarization rotation, vector field steering, phase change metasurface

1 Introduction

The polarization rotation and optical vortex (OV) characteristic of light are key to investigate the light–matter interaction. The ability to generate and manipulate arbitrary polarization states and orbital angular momentum (OAM) of light is of great significance in the applications of optical detection, biomedicine, optical communications and other fields [1–4]. Conventionally, anisotropic crystalline or chiral optical materials are utilized to manipulate the polarization of light based on their different optical responses of left-handed circularly polarized (LCP) light and right-handed circularly polarized (RCP) light [5, 6]. Spatial light modulators and q-plates [7, 8] are utilized to generate OV beams. However, the polarization rotation devices and the OV devices are bulky and lack of design flexibility, thus hindering the miniaturization and integration of optical systems.

Metamaterials, which are composed of artificial subwavelength structures, have novel optical properties that cannot be found in natural materials. Metasurfaces, known as two-dimensional (2D) matematerials, have attracted extensive attentions for the capability of controlling the light at-will, compact size and high efficiency [9, 10]. The flexible design strategies of the structures and the ability to manipulate light at subwavelength scale make them good candidates for integrated photonic devices with excellent performance, including polarization control devices [11, 12], holographic imaging [13], metalens [14], and so on. Metasurface for polarization conversion

Higher Education Press

https://doi.org/10.1007/s11467-022-1214-x

and vector beam generation is a hot topic in recent years [15–20]. Despite many efforts have been made to manipulate the polarization of light based on metasurfaces, there are still challenges in the construction of dynamic devices, especially in realizing multi-state polarization modulation and multifunctional optical devices.

Optical phase-change materials (PCMs) are considered as promising candidates to achieve dynamic optical devices [21, 22]. Compared with the weak effect of flexible or physically changeable materials [23, 24], the PCMs can effectively modulate light due to the large refractive index contrast between amorphous state (A-state) and crystalline state (C-state). In addition, the ultra-high switching speed of up to 10^9 Hz is also eye-catching [25–27]. To date, metasurfaces related to PCMs have been extensively researched in modulating the amplitude, phase, and polarization of light [28–33], which gives opportunities to develop dynamic optical devices at nanoscale. Integrating multiple functions into a single device is of great significance for promoting the practical application of integrated optics.

In this paper, the dynamically tunable polarization controller and OAM generator are implemented by using a metasurface based on typical phase-change material $Ge_2Sb_2Te_5$ (GST). The metsurface is composed of periodic supercell with four different GST elliptic cylinders located on a SiO_2 substrate. The phase state of each elliptic cylinder can be tuned independently between the A-state and C-state, resulting in different combinations of the elliptic cylinders state of the supercell, thus achieving multiple optical responses to incident light. By selectively controlling the phase transitions of the GST elliptic cylinders through external stimuli within the supercell, the polarization orientation of the transmitted light can be tuned to different angles that cover from 19.8° to 154.9° under normal incident linearly polarized (LP) light at a wavelength of 1550 nm. In addition to being a polarization rotator, the metasurface can also be used for an orbital angular momentum (OAM) generator. This work lays a foundation for dynamically controlling the polarization state of light and designing multifunctional dynamically tunable optical devices.

2 Proposed geometry and methods

The designed metasurface [Fig. 1(a)] is composed of supercells [Fig. 1(b)] all of a specified period P_2 and consisting of four-unit cells of period P_1. Each unit cell [Fig. 1(c)] consists of an elliptic GST cylinder on a square SiO_2 substrate. The GST elliptic cylinders have the same height h, a different semi-minor axis a and semi-major axis b. The angle between the semi-major axis and the x-axis is θ. By arranging the supercell periodically and tuning the state of each elliptic cylinder selectively, a meta-device with tunable optical activity

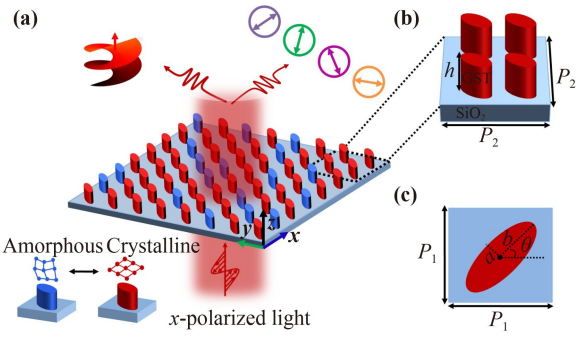

Fig. 1 Schematics of **(a)** the designed metasurface for polarization rotation and vector field steering, **(b)** the configuration of the supercell, and **(c)** top view of a unit cell.

can be realized and an OAM beam can be generated.

For each unit cell with GST elliptic cylinder, the Jones matrix can be expressed as

$$\mathrm{M}(\theta)=\begin{pmatrix}\cos\theta & -\sin\theta\\ \sin\theta & \cos\theta\end{pmatrix}\begin{pmatrix}p_1 & 0\\ 0 & p_2\end{pmatrix}\begin{pmatrix}\cos\theta & \sin\theta\\ -\sin\theta & \cos\theta\end{pmatrix}, \tag{1}$$

with $p_1 = e^{i\varphi_1}$ and $p_2 = e^{i\varphi_2}$ to be the complex transmission coefficients along semi-major axis and semi-minor axis. Here, φ_1 and φ_2 are the phases.

When the incident light is x-polarized and θ=45°, the transmitted light can be written as

$$\begin{pmatrix}E_x\\ E_y\end{pmatrix}=\frac{1}{2}\begin{pmatrix}p_1+p_2 & p_1-p_2\\ p_1-p_2 & p_1+p_2\end{pmatrix}\begin{pmatrix}1\\ 0\end{pmatrix}=\frac{1}{2}\begin{pmatrix}p_1+p_2\\ p_1-p_2\end{pmatrix}, \tag{2}$$

with $\varphi_1 - \varphi_2 = 0$, the transmitted light is x-polarized, while for $\varphi_1 - \varphi_2 = \pi$, the transmitted light is y-polarized, which means that Eq. (2) can be expressed as a Jones vector for elliptically polarized light, namely,

$$\begin{pmatrix}E_x\\ E_y\end{pmatrix}=\begin{pmatrix}t_x e^{i\delta_x}\\ t_y e^{i\delta_y}\end{pmatrix}. \tag{3}$$

Here, t_x and t_y represent amplitudes, and δ_x and δ_y represent phases.

Since the phase states of GST can transition freely between A- and C-states, multiple unit cells can be combined to generate multiple combinations of states to achieve different transmitted light. Here we only consider A-state and C-state of GST with optical refractive indexes $n_{\text{A-GST}} = 4.19 + 0.07\text{i}$ and $n_{\text{C-GST}} = 7.02 + 1.12\text{i}$ respectively [27], and investigate four unit cells in a supercell of the metasurface. The total electric field of the supercell is composited by

$$\begin{pmatrix}E_x'\\ E_y'\end{pmatrix}=\begin{pmatrix}\sum_{m=1}^{4} t_{xm}e^{i\delta_{xm}}\\ \sum_{m=1}^{4} t_{ym}e^{i\delta_{ym}}\end{pmatrix}=\begin{pmatrix}T_x e^{i\varphi_x}\\ T_y e^{i\varphi_y}\end{pmatrix}, \tag{4}$$

where T_x and T_y represent the amplitudes, and φ_x and φ_y represent the phases of the total electric field component

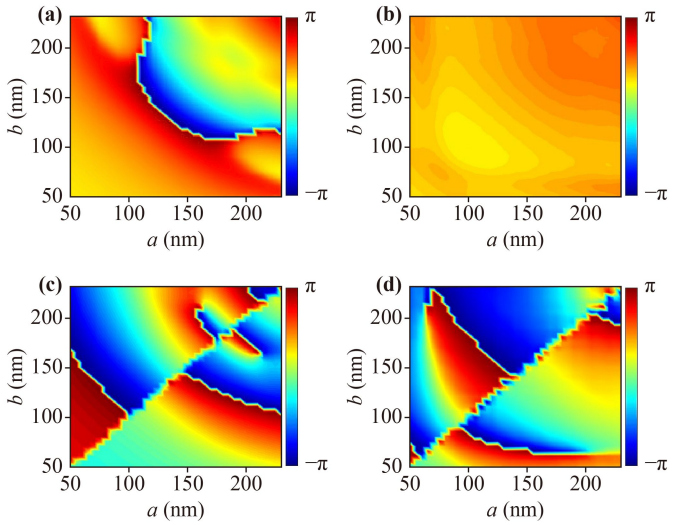

Fig. 2 Calculated phase of the coefficient of transmission t_{xx} in the A-state **(a)** and C-state **(b)**, and of t_{yx} in the A-state **(c)** and C-state **(d)** for a periodic unit-cell array at wavelength 1550 nm.

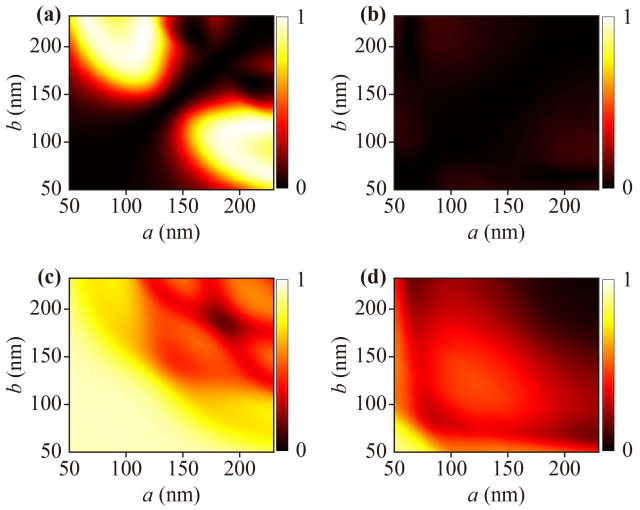

Fig. 3 Calculated PCR in **(a)** the A-state and **(b)** C-state, and transmittance in **(c)** the A-state and **(d)** C-state for a periodic unit cell array at wavelength 1550 nm.

$E_x^{'}$ and $E_y^{'}$ respectively. The corresponding polarization ellipse is [34]

$$\left(\frac{E_x^{'}}{T_x}\right)^2+\left(\frac{E_y^{'}}{T_y}\right)^2-2\left(\frac{E_x^{'}}{T_x}\right)\left(\frac{E_y^{'}}{T_y}\right)\cos\left(\varphi_y-\varphi_x\right)=\sin^2\left(\varphi_y-\varphi_x\right), \tag{5}$$

when $\varphi_y-\varphi_x=0$ or π, LP light can be achieved.

Assuming that x-polarized and y-polarized transmitted light can be obtained from each A-state and C-state unit cell respectively, it is possible to obtain transmitted light with 16 different polarization states from the periodically arranged supercell composed of four unit cells with different geometric parameters. Using the commercially available finite-difference time-domain (FDTD) simulations software (Ansys/Lumerical FDTD Solutions), the optical responses of a unit cell under normal-incident x-directed LP light at wavelength 1550 nm were investigated. Periodic boundary conditions were applied along the x and y directions, whereas perfectly matched layer conditions were employed along z direction. The height of each elliptic cylinder was fixed at $h=800$ nm and the period of the unit cell was fixed at $P_1=500$ nm, thus, the period of the supercell is P_2=1000 nm.

3 Results and discussion

By sweeping the semi-minor axis a and semi-major axis b of an elliptic cylinder, the phases (φ_{xx_A}, φ_{yx_A} and φ_{xx_C}, φ_{yx_C}) of the coefficients of transmission t_{xx} and t_{yx} were calculated for both the A- and C-states of GST [Figs. 2(a, c) and (b, d)] under x-LP light. The polarization conversion ratio (PCR, defined as $PCR=t_{yx}^2/(t_{xx}^2+t_{yx}^2)$, with t_{xx} and t_{yx} the co- and cross-polarization coefficients of transmission, respectively) and the transmissivity of the bi-states unit cells are also displayed [Figs. 3(a, b) and (c, d)]. In this work, one supercell composed of four different elliptical GST nano-pillars (for each nano-pillars, the transmitted light is x-polarized light for C-state and y-polarized light for A-state) were designed to obtain 16 different transmitted LP states, which means that the designed unit cells should meet the conditions that the PCR value in Fig. 3(a) should be close to 1 while the PCR value in Fig. 3(b) should be close to 0. Meanwhile, to ensure the high efficiency of the designed device, the transmittance of the selected unit cells should be as high as possible in both A- and C-states [Figs. 3(c, d)]. In addition, to ensure that the transmitted light remains linearly polarized for the periodically supercell with arbitrary meta-atom combined with other meta-atoms no matter it is A-state or C-state. According to Eq. (5), condition $\varphi_{yx\_A}-\varphi_{xx\_C}=\boldsymbol{\pi}$ is used. In theory, by considering supercells composed of four different elliptic cylinders with two states, the proposed metasurface has a total of 16 combinations of phase states, leading to 16 different transmitted light fields.

From the simulated results, values from the structural and corresponding optical-response parameters for the four-unit cells were selected (Table 1). The PCR of the selected elliptic cylinders are all above 90% in the A-state and below 2.5% in the C-state, indicating that the transmitted light is y-polarized in the A-state and x-polarized in the C-state illuminated by normal-incident x-polarized LP light. The absolute phase difference between the transmitted y-polarized and x-polarized light in the A-state and the C-state is smaller than 0.06 rad, indicating that LP transmitted light can be

Table 1 Selected settings of the structural and optical-response parameters.

Parameters	Values			
[a ,b] (nm)	[70 , 200]	[70, 205]	[65, 220]	[65, 225]
$PCR_{\_A}$	90.06%	93.81%	96.59%	97.57%
$PCR_{\_C}$	2.3%	2.48%	0.40%	0.69%
$\varphi_{yx\_A} - \varphi_{xx\_C}$ (rad)	–0.057	0.026	–0.05	0.006
$T_{\_A}$	74.05%	73.28%	73.52%	73.21%
$T_{\_C}$	22.34%	20.57%	18.26%	17.17%

produced. In addition, the transmittance of the selected structures is relatively high in the A-state but relatively lower in the C-state. This behavior is reasonable because the imaginary part of the GST refractive index is relatively larger in the C-state, leading to a larger optical loss.

Although the supercell contains four different elements, the coupling between adjacent elements is weak therefore neglected (see Fig. S1, Supporting Information). To investigate the performance of the dynamically tunable polarization rotator, the degree of linear polarization (*DoLP*) of the transmitted light, which describes the purity of LP light, is given in terms of the Stokes parameters. Specifically, $DoLP = \sqrt{S_1^2 + S_2^2}/S_0$, with S_0, S_1, and S_2 denoting the Stokes parameters [16]. Of the 16 possible combinations, eight state combinations were carefully selected [Fig. 4(a)] to disperses the polarization angle θ ($\theta = \arctan(|E_y| / |E_x|)$) to eight levels, covering a range from 19.8° to 154.9° [Fig. 4(b)]. The corresponding *DoLP* of the metasurfaces for these eight state combinations [Fig. 4(c)] are all above 0.88, demonstrating that the transmitted light is highly pure LP light. Furthermore, the calculated absolute ellipticity angle χ ($2\chi = \arcsin(S_3/S_0)$) [35] are below 15° [Fig. 4(d)], which verify that the transmitted lights from these unit cells are all nearly linearly polarized. The total efficiency of each state of the eight metasurfaces, which is defined as the ratio of the power of the transmitted light to that of incident light, is also presented [Fig. 4(e)]. The maximize transmittance approaches 73.6%, and the lowest efficiency of the metasurface is 16.9% ($N = 6$).

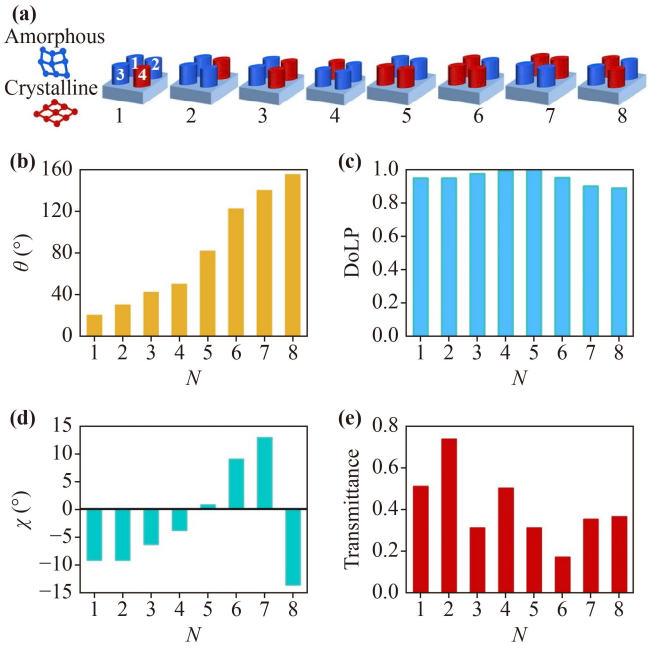

Fig. 4 **(a)** Configuration of GST states, **(b)** the polarization angle, **(c)** *DoLP*, **(d)** ellipticity angle and **(e)** transmittance of the transmitted light of the metasurface for each of the eight combination of unit cell from four elliptic cylinders (wavelength: 1550 nm).

In addition to being an optical rotator, the metasurface with the same supercell can also be used to generate optical vortex beams with OAM, which has novel application prospects in fields such as optical tweezers, optical information transmission and processing [36, 37]. According to the simulated results, supercell combing one C-state elliptic cylinder (C_1) and three A-state elliptic cylinders (A_2,A_3,A_4) can rotate the normal incident x-polarized light into transmitted light with a polarization angle of 49.59° ($N = 4$, labeled as G_4), while supercell combing two C-state elliptic cylinders (C_1,C_2) and two A-state elliptic cylinders (A_3,A_4) can rotate the normal incident x-polarized light into transmission light with polarization angle of 139.60° ($N = 7$, labeled as G_7) [Fig. 4(a)]. Since the polarization states are almost orthogonal and high transmission intensity contrast can be achieved with a 50° or 140° polarizer placed on the output path, we believe that the proposed metasurface can be used to construct a fork-shaped structure to generate optical vortex beam with OAMs by reasonably arranging the G_4 and G_7 states of the supercells. Figure 5(a) shows the process of obtaining the required phase arrangement to generate optical vortex beams with topological charges of –1, 0 and 1. First, the phase of Laguerre-Gaussian beam LG_{pl} [38] with azimuthal index $l = 1$, radial index $p = 0$ and waist radius to be 25 μm was obtained, and then the phase was superimposed with the phase of a tilted plane wave $Ae^{i\varphi}$ (with amplitude $A = 1$ and phase φ form $-\pi$ to π). Finally, the fork-shaped phase profile was obtained by discretizing the superimposed phase to binary codes "0" and "1". By encoding G_7 to "0" and G_4 to "1 ", metasurface with 80×80 supercells (80 μm× 80 μm) was simulated under normally incident x-polarized light. In Fig. (5), the 50° polarizer was used to filter the transmitted light with a polarization angle of 50° and

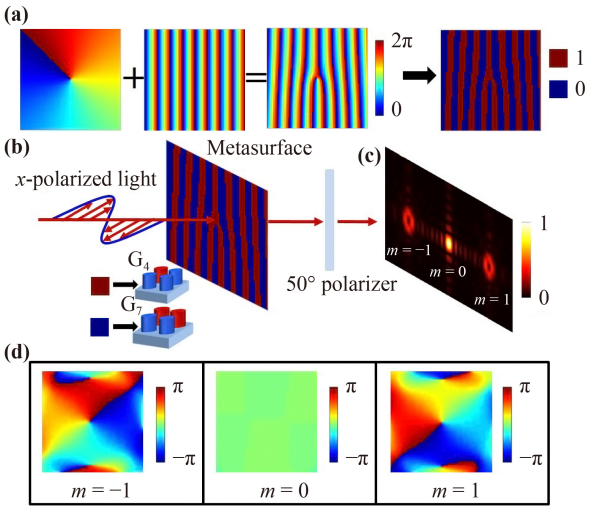

Fig. 5 **(a)** Procedure to obtain the required phase arrangement to generate optical vortex beam. **(b)** Schematic diagram for obtaining optical vortex beam with OAMs using GST metasurface. The calculated distributions of **(c)** intensity and **(d)** phase of the diffraction beam at a transverse plane of $z = 400$ mm (wavelength: 1550 nm).

block the transmitted light with other polarization angles at the same time, as shown in Fig. 5(b). The calculated far-field intensity of the diffraction beam at a transverse plane of $z = 400$ mm are shown in Fig. 5(c). The corresponding phase distributions are shown in Fig. 5(d). According the simulated results, we can conclude that an optical vortex beam carrying the 0th-, 1st-, and –1st-order OAMs has been successfully generated.

The numerical simulation of the designed metasurface proves that it is possible to achieve multi-state tunable optical activity and optical vortex beam with OAM in a single device. Although the corresponding experiment has not been performed due to the limited condition, it is expected to be realized in the future. Metasurface with 600-nm-thick GST has been demonstrated theoretically and experimentally with the phase change from A- to C-state [30]. By using an artificial neural network (ANN) and training spectra predicting network (SPN) networks, metasurface consisting of GST cylinders with thickness vary from 0.05 μm to 1 μm has been reported theoretically [39]. Although metasurfaces with 800-nm-thick GST has not yet been demonstrated, GST films with different thicknesses (up to 1.5 μm) have been obtained experimentally [40–42], indicating possibilities to achieve 800-nm-thick GST nanocylinders.

The selective modulation of GST metasurface has also been reported [43], and there are several available matured techniques to realize the independent modulation of the GST nanocylinders such as laser-direct writing [44] and conductive-atomic force microscopy (C-AFM) [45, 46]. For the method of laser-direct writing, each nanocylinder requires different pulse energy, and a displacement platform with high accuracy is needed to gradually control the displacement of nanocylinder so that the phases of nanocylinders can be changed one by one. While for the method of C-AFM, the GST nanocylinders are deposited on the electrodes, and the phase transitions of the nanocylinders are achieved by applying electric current pulses. Theoretically, the transition between the two phase states of the phase change materials is in ultra-high speed, and the switching time can be down to few nanoseconds. However, the proposed metasurface-based devices are composed of four meta-atoms, the switching of the device requires to address each meta-atom independently, resulting in a complex electrodes design and manufacture procedures. The alternative switching method is using a femtosecond laser pulse to induce the phase transition between the two phase states, and addressing each meta-atom one by one is quite time consuming which dramatically reduces the switching speed. Simple, less manufacturing complexity and effective ways still need to be explored.

4 Conclusions

In conclusion, we proposed a multi-states tunable metasurface based on the phase-change material GST. The supercell of the metasurface contains four elliptic cylinders made of GST that differ in the length of the semi-minor and semi-major axes. The phase state of each elliptic cylinders can be independently tuned between A- and C-states. From the simulated results, we confirmed that the proposed metasurface can act as a dynamically tunable polarization rotator, which can rotate the normal-incident LP light by an angle covering a range from 19.8° to 154.9° at a wavelength of 1550 nm. Moreover, the metasurface also enables function of OAM beam generation. The designed metasurface has potential applications in areas such as imaging and optical communication. This work will shed light on designing miniature and integrated devices that own dynamic multiply functionalities.

Electronic supplementary material Supplementary materials are available in the online version of this article at https://doi.org/10.1007/s11467-022-1214-x and https://journal.hep.com.cn/fop/EN/10.1007/s11467-022-1214-x and are accessible for authorized users.

Author contributions H.H. designed and simulated the structure. The project was conceived and supervised by Z.X. and X.Y.. All authors analyzed and discussed the results and approved it for publication.

Data availability Data underlying the results presented in this paper are not publicly available at this time but can be obtained from the authors upon reasonable request.

Conflict of interest The authors declare that the research was conducted in the absence of any commercial or financial relationships that could be constructed as a potential conflict of interest.

Acknowledgements We are grateful for financial supports from the Guangdong Major Project of Basic Research (Grant No. 2020B0301030009), the National Key R&D Program of China (Grant No. 2018YFB1801801), the National Natural Science Foundation of China (Grant Nos. 61935013, 61975133, 11947017, and 12104318), the Natural Science Foundation of Guangdong Province (Grant No. 2020A1515011185), the Science and Technology Innovation Commission of Shenzhen (Grant Nos. KQTD20170330110444030, JCYJ2018 0507182035270, and JCYJ20200109114018750), Shenzhen University (Grant No. 2019075), and China Postdoctoral Science Foundation (Grant No. 2021T140470).

References

1. H. Rhee, Y. G. June, J. S. Lee, K. K. Lee, J. H. Ha, Z. H. Kim, S. J. Jeon, and M. Cho, Femtosecond characterization of vibrational optical activity of chiral molecules, *Nature* 458(7236), 310 (2009)
2. E. Bahar, Road maps for the use of Mueller matrix measurements to detect and identify biological and chemical materials through their optical activity: Potential applications in biomedicine, biochemistry, security, and industry, *J. Opt. Soc. Am. B* 26(2), 364 (2009)
3. Y. He, W. Bo, R. K. Dukor, and L. A. Nafie, Determination of absolute configuration of chiral molecules using vibrational optical activity: A review, *Appl. Spectrosc.* 65(7), 699 (2011)
4. Y. Lian, X. Qi, Y. Wang, Z. Bai, Y. Wang, and Z. Lu, OAM beam generation in space and its applications: A review, *Opt. Lasers Eng.* 151, 106923 (2022)
5. E. Arbabi, A. Arbabi, S. M. Kamali, Y. Horie, and A. Faraon, Multiwavelength polarization-insensitive lenses based on dielectric metasurfaces with meta-molecules, *Optica* 3(6), 628 (2016)
6. V. Sharma, M. Crne, J. O. Park, and M. Srinivasarao, Structural origin of circularly polarized iridescence in jeweled beetles, *Science* 325(5939), 449 (2009)
7. F. Cardano, E. Karimi, S. Slussarenko, L. Marrucci, C. de Lisio, and E. Santamato, Polarization pattern of vector vortex beams generated by q-plates with different topological charges, *Appl. Opt.* 51(10), C1 (2012)
8. Y. S. Rumala, G. Milione, T. A. Nguyen, S. Pratavieira, Z. Hossain, D. Nolan, S. Slussarenko, E. Karimi, L. Marrucci, and R. R. Alfano, Tunable supercontinuum light vector vortex beam generator using a q-plate, *Opt. Lett.* 38(23), 5083 (2013)
9. S. M. Kamali, E. Arbabi, A. Arbabi, and A. Faraon, A review of dielectric optical metasurfaces for wavefront control, *Nanophotonics* 7(6), 1041 (2018)
10. K. Ding, S. Y. Xiao, and L. Zhou, New frontiers in metamaterials research: Novel electronic materials and inhomogeneous metasurfaces, *Front. Phys.* 8(4), 386 (2013)
11. A. H. Dorrah, N. A. Rubin, A. Zaidi, M. Tamagnone, and F. Capasso, Metasurface optics for on-demand polarization transformations along the optical path, *Nat. Photonics* 15(4), 287 (2021)
12. Z. Y. Song, Q. Q. Chu, X. P. Shen, and Q. H. Liu, Wideband high-efficient linear polarization rotators, *Front. Phys.* 13(5), 137803 (2018)
13. D. Wen, J. J. Cadusch, J. Meng, and K. B. Crozier, Light field on a chip: Metasurface-based multicolor holograms, *Adv. Photonics* 3(2), 024001 (2021)
14. M. K. Chen, Y. Wu, L. Feng, Q. Fan, M. Lu, T. Xu, and D. P. Tsai, Principles, functions, and applications of optical meta-lens, *Adv. Opt. Mater.* 9(4), 2001414 (2021)
15. H. Yang, Z. Xie, G. Li, K. Ou, F. Yu, H. He, H. Wang, and X. Yuan, All-dielectric metasurface for fully resolving arbitrary beams on a higher-order Poincaré sphere, *Photon. Res.* 9(3), 331 (2021)
16. Z. Li, X. Cai, L. Huang, H. Xu, Y. Wei, and N. Dai, Controllable polarization rotator with broadband high transmission using all-dielectric metasurfaces, *Adv. Theory Simul.* 2(9), 1900086 (2019)
17. D. Wen, F. Yue, C. Zhang, X. Zang, H. Liu, W. Wang, and X. Chen, Plasmonic metasurface for optical rotation, *Appl. Phys. Lett.* 111(2), 023102 (2017)
18. M. A. Cole, W. C. Chen, M. Liu, S. S. Kruk, W. J. Padilla, I. V. Shadrivov, and D. A. Powell, Strong broadband terahertz optical activity through control of the Blaschke phase with chiral metasurfaces, *Phys. Rev. A* 8(1), 014019 (2017)
19. M. Al-Mahmoud, V. Coda, A. Rangelov, and G. Montemezzani, Broadband polarization rotator with tunable rotation angle composed of three wave plates, *Phys. Rev. A* 13(1), 014048 (2020)
20. H. Ahmed, H. Kim, Y. Zhang, Y. Intaravanne, J. Jang, J. Rho, S. Chen, and X. Chen, Optical metasurfaces for generating and manipulating optical vortex beams, *Nanophotonics* 11(5), 941 (2022)
21. Y. Zhang, C. Ríos, M. Y. Shalaginov, M. Li, A. Majumdar, T. Gu, and J. Hu, Myths and truths about optical phase change materials: A perspective, *Appl. Phys. Lett.* 118(21), 210501 (2021)
22. F. Ding, Y. Yang, and S. I. Bozhevolnyi, Dynamic metasurfaces using phase-change chalcogenides, *Adv. Opt. Mater.* 7(14), 1801709 (2019)
23. I. Zubritskaya, N. Maccaferri, X. Inchausti Ezeiza, P. Vavassori, and A. Dmitriev, Magnetic control of the chiroptical plasmonic surfaces, *Nano Lett.* 18(1), 302 (2018)
24. H. S. Ee and R. Agarwal, Tunable metasurface and flat optical zoom lens on a stretchable substrate, *Nano Lett.* 16(4), 2818 (2016)
25. J. Kalikka, J. Akola, and R. O. Jones, Simulation of crystallization in $Ge_2Sb_2Te_5$: A memory effect in the canonical phase-change material, *Phys. Rev. B* 90(18), 184109 (2014)
26. D. Loke, T. H. Lee, W. J. Wang, L. P. Shi, R. Zhao, Y. C. Yeo, T. C. Chong, and S. R. Elliott, Breaking the speed limits of phase-change memory, *Science* 336(6088), 1566 (2012)
27. M. Wuttig, H. Bhaskaran, and T. Taubner, Phase-change materials for non-volatile photonic applications, *Nat. Photonics* 11(8), 465 (2017)
28. J. Tian, H. Luo, Y. Yang, F. Ding, Y. Qu, D. Zhao, M. Qiu, and S. I. Bozhevolnyi, Active control of anapole states by structuring the phase-change alloy $Ge_2Sb_2Te_5$, *Nat. Commun.* 10(1), 396 (2019)

29. C. Choi, S. Y. Lee, S. E. Mun, G. Y. Lee, J. Sung, H. Yun, J. H. Yang, H. O. Kim, C. Y. Hwang, and B. Lee, Metasurface with nanostructured $Ge_2Sb_2Te_5$ as a platform for broadband-operating wavefront switch, *Adv. Opt. Mater.* 7(12), 1900171 (2019)
30. S. Abdollahramezani, O. Hemmatyar, H. Taghinejad, A. Krasnok, Y. Kiarashinejad, M. Zandehshahvar, A. Alù, and A. Adibi, Tunable nanophotonics enabled by chalcogenide phase-change materials, *Nanophotonics* 9(5), 1189 (2020)
31. M. Zhang, M. Pu, F. Zhang, Y. Guo, Q. He, X. Ma, Y. Huang, X. Li, H. Yu, and X. Luo, Plasmonic metasurfaces for switchable photonic spin-orbit interactions based on phase change materials, *Adv. Sci. (Weinh.)* 5(10), 1800835 (2018)
32. X. Yin, T. Steinle, L. Huang, T. Taubner, M. Wuttig, T. Zentgraf, and H. Giessen, Beam switching and bifocal zoom lensing using active plasmonic metasurfaces, *Light Sci. Appl.* 6(7), e17016 (2017)
33. B. Fang, D. Feng, P. Chen, L. Shi, J. Cai, J. Li, C. Li, Z. Hong, and X. Jing, Broadband cross-circular polarization carpet cloaking based on a phase change material metasurface in the mid-infrared region, *Front. Phys.* 17(5), 53502 (2022)
34. B. J. Thompson, D. Goldstein, and D. H. Goldstein, Polarized Light, Revised and Expanded, 2nd Ed., 42–43, CRC Press, 2003
35. L. Cong, W. Cao, X. Zhang, Z. Tian, J. Gu, R. Singh, J. Han, and W. Zhang, A perfect metamaterial polarization rotator, *Appl. Phys. Lett.* 103(17), 171107 (2013)
36. J. Chen, C. Wan, and Q. Zhan, Engineering photonic angular momentum with structured light: A review, *Adv. Photonics* 3(6), 064001 (2021)
37. Y. Shen, X. Wang, Z. Xie, C. Min, X. Fu, Q. Liu, M. Gong, and X. Yuan, Optical vortices 30 years on: OAM manipulation from topological charge to multiple singularities, *Light Sci. Appl.* 8(1), 90 (2019)
38. D. Naidoo, K. Aït-Ameur, M. Brunel, and A. Forbes, Intra-cavity generation of superpositions of Laguerre-Gaussian beams, *Appl. Phys. B* 106(3), 683 (2012)
39. J. R. Thompson, J. A. Burrow, P. J. Shah, J. Slagle, E. S. Harper, A. Van Rynbach, I. Agha, and M. S. Mills, Artificial neural network discovery of a switchable metasurface reflector, *Opt. Express* 28(17), 24629 (2020)
40. N. Fleurence, B. Hay, G. Davée, A. Cappella, and E. Foulon, Thermal conductivity measurements of thin films at high temperature modulated photothermal radiometry at LNE, *Phys. Status Solidi. A* 212(3), 535 (2015)
41. S. C. Agarwal, Role of potential fluctuations in phase-change GST memory devices, *Phys. Status Solidi B* 249(10), 1956 (2012)
42. S. W. Ryu, J. H. Oh, J. H. Lee, B. J. Choi, W. Kim, S. K. Hong, C. S. Hwang, and H. J. Kim, Phase transformation behaviors of SiO_2 doped $Ge_2Sb_2Te_5$ films for application in phase change random access memory, *Appl. Phys. Lett.* 92(14), 142110 (2008)
43. C. H. Chu, M. L. Tseng, J. Chen, P. C. Wu, Y. H. Chen, H. C. Wang, T. Y. Chen, W. T. Hsieh, H. J. Wu, G. Sun, and D. P. Tsai, Active dielectric metasurface based on phase-change medium, *Laser Photonics Rev.* 10(6), 986 (2016)
44. Q. Wang, E. T. F. Rogers, B. Gholipour, C. M. Wang, G. Yuan, J. Teng, and N. I. Zheludev, Optically reconfigurable metasurfaces and photonic devices based on phase change materials, *Nat. Photonics* 10(1), 60 (2016)
45. R. Pandian, B. J. Kooi, G. Palasantzas, J. T. M. De Hosson, and A. Pauza, Nanoscale electrolytic switching in phase-change chalcogenide films, *Adv. Mater.* 19(24), 4431 (2007)
46. W. Zhang, R. Mazzarello, M. Wuttig, and E. Ma, Designing crystallization in phase-change materials for universal memory and neuro-inspired computing, *Nat. Rev. Mater.* 4(3), 150 (2019)